

Light-induced thermal noise *anomaly* governed by quantum metric

Longjun Xiang,¹ Lei Zhang,^{2,*} Jun Chen,³ Fuming Xu,¹ Yadong Wei,¹ and Jian Wang^{1,4,†}

¹College of Physics and Optoelectronic Engineering, Shenzhen University, Shenzhen 518060, China

²State Key Laboratory of Quantum Optics and Quantum Optics Devices,
Institute of Laser Spectroscopy, Shanxi University, Taiyuan 030006, China

³State Key Laboratory of Quantum Optics and Quantum Optics Devices,
Institute of Theoretical Physics, Shanxi University, Taiyuan 030006, China

⁴Department of Physics, University of Hong Kong, Pokfulam Road, Hong Kong, P. R. China

(Dated: December 18, 2024)

Traditionally, thermal noise in electric currents, arising from thermal agitation, is expected to increase with temperature T and disappear as T approaches zero. Contrary to this expectation, we discover that the resonant DC thermal noise (DTN) in photocurrents not only persists at $T = 0$ but also exhibits a divergence proportional to $1/T$. This thermal noise *anomaly* arises from the unique electron-photon interactions near the Fermi surface, manifesting as the interplay between the inherent Fermi-surface property and the resonant optical selection rules of DTN, and thereby represents an unexplored noise regime. Notably, we reveal that this *anomalous* DTN, especially in time-reversal-invariant systems, is intrinsically linked to the quantum metric. We illustrate this *anomalous* DTN in massless Dirac materials, including two-dimensional graphene, the surfaces of three-dimensional topological insulators, and three-dimensional Weyl semimetals, where the quantum metric plays a pivotal role. Finally, we find that the total noise spectrum at low temperatures, which includes both the DC shot noise and the *anomalous* DTN, will universally peak at $\omega_p = 2|\mu|$ with ω_p the frequency of light and μ the chemical potential of the bulk crystals.

Introduction. — Quantum fluctuations, manifesting as quantum noise, are ubiquitous in transport processes and are well understood in mesoscopic conductors¹⁻³. Among these, shot noise (SN) in mesoscopic systems, arising from charge quantization, is considered the dominant source of noise at low temperatures^{3,4}. Oppositely, thermal noise (TN), driven by thermal agitation, becomes the prevailing source of quantum noise at high temperatures and disappears at low temperatures^{3,5}.

Beyond mesoscopic conductors, the SN of electric current in bulk crystals under a static electric field is closely tied to the quantum metric of Bloch electrons⁶. Meanwhile, the TN of current in similar scenarios can manifest as an intrinsic Hall signature, even in time-reversal-invariant systems⁷. Additionally, the DC shot noise (DSN) of photocurrent in bulk crystals under optical electric fields has been developed as a tool to probe the quantum geometric properties of centrosymmetric quantum materials^{8,9}. However, the DC thermal noise (DTN) of photocurrent in bulk crystals under optical electric fields remains unexplored, leaving a critical gap in understanding the quantum noise of bulk crystals under light irradiation.

In this *Letter*, we develop the quantum theory of DTN for photocurrent in bulk crystals under an optical electric field. We demonstrate that the DTN in time-reversal-invariant systems is intimately related to the quantum metric, which as the quantum geometric origin of the intrinsic nonlinear Hall effect recently received significant attention¹⁰⁻¹⁷. Remarkably, unlike the TN occurred in mesoscopic conductors and in bulk crystals under static electric fields, we discover that the DTN not only persists at zero temperature ($T = 0$) but also can exhibit a divergent $1/T$ behavior. This thermal noise *anomaly* arises from the distinctive electron-photon interactions near the Fermi surface, essentially due to the interplay between the inherent Fermi-surface property and the optical selection rule of DTN. This phenomenon thus unveils a novel

quantum noise regime. To illustrate our proposals, we investigate the *anomalous* DTN in quantum materials with a nontrivial quantum metric, including two-dimensional (2D) graphene¹⁸⁻²¹, the surface of three-dimensional (3D) topological insulators²²⁻²⁷, and 3D Weyl semimetals²⁸⁻³⁰. Finally, we show that the total noise spectrum at low temperatures, which contains both the DSN and the *anomalous* DTN, will universally peak at $\omega_p = 2|\mu|$, where ω_p is the frequency of optical electric fields and μ is the chemical potential of the bulk crystals.

Unique electron-photon interaction. — In mesoscopic physics, it is well established that the TN of electric current vanishes at zero temperature. Specifically, in a two-terminal mesoscopic conductor, the TN, applicable in both linear and nonlinear regimes, can be expressed as^{3,31} ($e = \hbar = k_B = 1$)

$$S_T = \frac{1}{\pi} \sum_{\alpha,n} \int_E f_{\alpha}(1 - f_{\alpha}) T_n = -\frac{T}{\pi} \sum_{\alpha,n} \int_E f'_{\alpha} T_n, \quad (1)$$

where $\int_E = \int dE$, $\alpha = \{L, R\}$ denotes the left and right electrodes, $T_n = T_n(E)$ stands for the transmission of the n th channel, $f_{\alpha} \equiv f(E, \mu_{\alpha})$ represents the equilibrium Fermi distribution function (Here E is the energy and μ_{α} is the chemical potential of the electrode α), and $f'_{\alpha} \equiv \partial f_{\alpha} / \partial E$. The presence of f'_{α} indicates that the TN is contributed by the electrons on the Fermi surface³². As a result, at $T = 0$ we find $f'_{\alpha} = -\delta(\mu_{\alpha} - E)$ and we arrive at

$$\lim_{T \rightarrow 0} S_T = \lim_{T \rightarrow 0} \frac{T}{\pi} \sum_{\alpha,n} T_n(\mu_{\alpha}) = 0 \quad (2)$$

since $\sum_{\alpha,n} T_n(\mu_{\alpha})$ is finite.

In bulk crystals, the noise of photocurrent generally is given

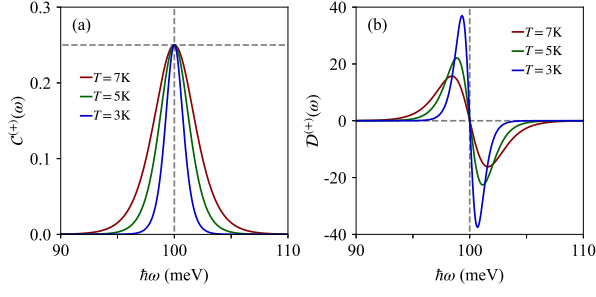


FIG. 1. The temperature and frequency dependencies of (a) $C^{(+)}$ and (b) $D^{(+)}$, as calculated in Eqs. (8-9), respectively. Here we have set $\mu = 50\text{meV}$ so that the resonant peaks appear near $\omega = 2\mu = 100\text{meV}$.

by⁹

$$\bar{S}_T = \frac{1}{2} \sum_{mn} \int_k J_{mn}^a J_{nm}^b (f_{nm}^2 + \bar{f}_{nm}). \quad (3)$$

Here $\int_k = 1/V \int d\mathbf{k}/(2\pi)^d$ with d and V being the spatial dimension and the volume of the system³³, respectively; J_{nm}^a is the matrix element of photocurrent operator; $f_{nm} = f_n - f_m$ and $\bar{f}_{nm} = f_n(1 - f_n) + f_m(1 - f_m)$, where $f_n \equiv f(\epsilon_n, \mu)$ represents the equilibrium Fermi distribution function but with ϵ_n being the energy of the n th Bloch band and μ being the chemical potential of the bulk crystal. In Eq. (3), the first term featuring the Fermi-sea property gives the DSN⁹ while the second term gives the DTN, which behaves as the Fermi-surface property like Eq. (1) due to $f_n(1 - f_n) = -T\partial f_n/\partial\epsilon_n = -Tf_n'$.

At the second order of optical electric fields and within the two-band limit^{8,35}, the resonant DTN of photocurrent in bulk crystals has two distinct contributions and can be formally expressed as [see Eqs. (11-12) derived below]:

$$\bar{S}_T^{(1)} = -T \int_k (f_n' + f_m') N_{nm}^{(1)} \delta(\omega - \omega_{mn}), \quad (4)$$

$$\bar{S}_T^{(2)} = -T \int_k \omega (f_n'' - f_m'') N_{nm}^{(2)} \delta(\omega - \omega_{mn}), \quad (5)$$

where $f_n'' \equiv \partial^2 f_n/\partial\epsilon_n^2$, ω is the frequency of the optical electric field, $\hbar\omega_{mn} = \epsilon_{mn} = \epsilon_m - \epsilon_n$, and $N_{nm}^{(1/2)}$ related to *quantum metric* will be calculated below. Compared to the TN described by Eq. (1), besides the delta function given by the inherent Fermi-surface property f_n' and f_n'' at zero temperature, we notice that the DTNs $\bar{S}_T^{(1/2)}$ contain an additional delta function $\delta(\omega - \omega_{mn})$ particularly due to the optical selection rule³⁶. Consequently, the conclusion implied by Eq. (2) is no longer hold since $\lim_{T \rightarrow 0} T \int_k f_n' = 0$ but $\lim_{T \rightarrow 0} T f_n'' \neq 0$ and $\lim_{T \rightarrow 0} T f_n'' \neq 0$ when the k -integral is killed by the additional optical selection rule.

Specifically, we take the two-band Dirac Hamiltonian into account^{37,38}

$$H = \mathbf{d} \cdot \boldsymbol{\sigma}, \quad (6)$$

whose band dispersions are given by $\epsilon_{\pm} = \pm d$, where $+$ ($-$) correspond to the upper (lower) band, respectively, and $d^2 = |\mathbf{d}|^2 = \sum_i d_i^2$ with d_i being the functions of \mathbf{k} . For this Hamiltonian, Eqs.(4-5) can be simplified to

$$\bar{S}_T^{(1)} = \mathcal{C}(\omega)\mathcal{N}^{(1)}, \quad \bar{S}_T^{(2)} = \mathcal{D}(\omega)\mathcal{N}^{(2)}, \quad (7)$$

where $\mathcal{N}^{(1/2)} \equiv \int_k N_{-+}^{(1/2)} \delta(\omega - 2d)$ are finite and independent of temperature, $\mathcal{C}(\omega) = \mathcal{C}^{(-)}(\omega) + \mathcal{C}^{(+)}(\omega)$ with $\mathcal{C}^{(\pm)}(\omega) \equiv -Tf_{\pm}'$ ³⁹ and $\mathcal{D}(\omega) = \mathcal{D}^{(-)}(\omega) - \mathcal{D}^{(+)}(\omega)$ with $\mathcal{D}^{(\pm)}(\omega) \equiv -\omega T f_{\pm}''$. Explicitly, they are given by⁴⁰

$$\mathcal{C}^{(\pm)} = \frac{1}{4} \text{sech}^2 \left(\frac{\hbar\omega \mp 2\mu}{4k_B T} \right), \quad (8)$$

$$\mathcal{D}^{(\pm)} = \frac{\mp \hbar\omega}{4k_B T} \text{sech}^2 \left(\frac{\hbar\omega \mp 2\mu}{4k_B T} \right) \tanh \left(\frac{\hbar\omega \mp 2\mu}{4k_B T} \right), \quad (9)$$

which are dimensionless universal functions of temperature, frequency, and chemical potential. Here \hbar and k_B are restored by dimension analysis. Note that $\mathcal{C}^{(\pm)}(\omega)$ exhibits a resonant peak at $\omega = 2|\mu|$, with a universal maximum value $1/4$, even in the limit as $T \rightarrow 0$, as shown in Fig. 1a for $\mathcal{C}^{(+)}(\omega)$. Consequently, $\bar{S}_T^{(1)}$ defines the first type of *anomalous* DTN. Furthermore, $\mathcal{D}^{(\pm)}(\omega)$ obtained by taking the derivative of $\mathcal{C}^{(\pm)}(\omega)$, gives two resonant peaks on either side of $\omega = 2|\mu|$, even in the limit as $T \rightarrow 0$, as shown in Fig. 1b for $\mathcal{D}^{(+)}(\omega)$. As a result, $\bar{S}_T^{(2)}$ defines the second type of *anomalous* DTN, characterized by a temperature dependence of $1/T$ [see Eq. (9)].

To close this section, we wish to conclude that the *anomalous* DTNs arise from the unique electron-photon interactions near the Fermi surface, which manifests as the interplay between the inherent Fermi-surface property f_n' or f_n'' and the resonant optical selection rule $\delta(\omega - \omega_{mn})$ of DTN — a phenomenon that can not be expected in mesoscopic conductors or in bulk crystals under a static electric field. Therefore, this thermal noise *anomaly* represents a novel quantum noise regime beyond the conventional thermal noise. Building on these qualitative insights, we proceed to develop the quantum theory for resonant DTN.

Quantum theory of DTN. — Similar to the DSN, the lowest-order DTN occurring at the second order of the optical electric field \mathbf{E} is given by⁹:

$$\bar{S}_T^{(2)} = \delta(\Omega_1) (\bar{\sigma}_{L/C} + \tau \bar{\eta}_{L/C}) \delta_{L/C}, \quad (10)$$

where Ω_1 represents the response frequency for $t - t'$, τ is the effective illumination time. The tensors $\bar{\sigma}$ and $\bar{\eta}$ denote the response coefficient for the shift and injection DTN, respectively. Here the shift (injection) DTN characterizes the quantum fluctuation of the shift (injection) photocurrent operator. Additionally, $\delta_L \equiv |\mathbf{E}|^2$ and $\delta_C \equiv |\mathbf{E} \times \mathbf{E}^*|$ correspond to linearly polarized light (LPL) and circularly polarized light (CPL), respectively. As indicated by the subscripts L and C of $\bar{\sigma}/\bar{\eta}$ in Eq.(10), we notice that both $\bar{\sigma}$ and $\bar{\eta}$ can be excited either by LPL or CPL, similar to the DSN⁹ and the DC photocurrent^{41,42}.

In time-reversal-invariant systems, which are the focus of this *Letter*, only the shift/injection DTN excited by CPL/LPL can appear⁴³. The shift DTNs excited by CPL feature the antisymmetric form, which disappears for the linear Dirac Hamiltonian⁴⁰. Consequently, we will concentrate on the injection DTN in the following. Specifically, the response tensors for injection DTN within the two-band limit are given by⁴⁰

$$\bar{\eta}_{L,1}^{abc} = -T \int_k (f'_n + f'_m) \Xi_{nm}^{abc} \delta(\omega - \omega_{mn}), \quad (11)$$

$$\bar{\eta}_{L,2}^{abc} = -T \int_k \omega (f''_n - f''_m) \Lambda_{nm}^{abc} \delta(\omega - \omega_{mn}), \quad (12)$$

where $\Xi_{nm}^{abc} = -\pi (\Delta_{nm}^a)^2 g_{nm}^{bc} / 2$ with $g_{nm}^{bc} = r_{nm}^b r_{mn}^c + r_{nm}^c r_{mn}^b$ being the quantum metric (Here r_{nm}^b is the interband Berry connection) and $\Delta_{nm}^a = v_n^a - v_m^a$ (Here $v_n^a \equiv \partial \epsilon_n / \partial k_a$ is the group velocity for the n th Bloch band). In addition, $\Lambda_{nm}^{abc} = \pi \Delta_{nm}^a (g_{nm}^{ac} v_n^b + g_{nm}^{ab} v_n^c) / 4$.

Several observations are in order. First, we note that $\bar{\eta}_{L,1}^{abc}$ and $\bar{\eta}_{L,2}^{abc}$ give rise to the first and second type of *anomalous* DTNs, respectively, resulting from the interplay between the Fermi-surface property and the optical selection rule discussed previously. Second, $\bar{\eta}_{L,1/2}^{abc}$ are symmetric with respect to indices b and c since the injection DTN is excited by LPL⁴¹. Third, we find that $\bar{\eta}_{L,1/2}^{abc}$ are \mathcal{T} -even tensors, since $\mathcal{T}v_n^a = -v_n^a$ and $\mathcal{T}g_{nm}^{bc} = g_{nm}^{bc}$, where \mathcal{T} denotes the time-reversal symmetry. Finally, for the two-band Dirac Hamiltonian Eq. (6), we find that Eqs. (11-12) can be similarly rewritten as

$$\bar{\eta}_{L,1}^{abc} = \mathcal{C}(\omega) \mathcal{N}_1^{abc}, \quad \bar{\eta}_{L,2}^{abc} = \mathcal{D}(\omega) \mathcal{N}_2^{abc}, \quad (13)$$

where $\mathcal{C}(\omega)$ and $\mathcal{D}(\omega)$ have been defined in Eq. (7) and

$$\mathcal{N}_1^{abc} \equiv \int_k \Xi_{-+}^{abc} \delta(\omega - 2d), \quad (14)$$

$$\mathcal{N}_2^{abc} \equiv \int_k \Lambda_{-+}^{abc} \delta(\omega - 2d). \quad (15)$$

Note that the quantum metric g_{-+}^{ab} ⁴⁴, appearing in both Ξ_{-+}^{abc} and Λ_{-+}^{abc} , plays a critical role in ensuring a nonvanishing *anomalous* DTN, as will be illustrated below. In addition, $\Xi_{nm}^{abc} E^b E^c = N_{nm}^{(1)}$, $\Lambda_{nm}^{abc} E^b E^c = N_{nm}^{(2)}$, $\mathcal{N}_1^{abc} E^b E^c = \mathcal{N}^{(1)}$, and $\mathcal{N}_2^{abc} E^b E^c = \mathcal{N}^{(2)}$.

Anomalous DTN in 2D. — We first explore the *anomalous* DTN in 2D monolayer graphene, where $\mathbf{d} = (k_x, k_y, 0)$ in Eq. (6) to capture its low-energy physics near \mathbf{K} or \mathbf{K}' point²¹. For this model, $\omega_{+-} = 2k$ with $k = (k_x^2 + k_y^2)^{1/2}$, $v_{\pm}^a = \pm k_a / k$, and $g_{\pm\pm}^{bc} = (k^2 \delta_{bc} - k_b k_c) / (2k^4)$. Using these expressions, along with Eqs. (14-15) the first and second *anomalous* DTNs can be calculated as

$$\bar{\eta}_{L,1}^{abb} = 3\bar{\eta}_{L,1}^{aaa} = -\frac{e^4 v_F^2}{\hbar^2 S} \frac{3\mathcal{C}(\omega)}{8\omega}, \quad a, b \in \{x, y\}, \quad (16)$$

$$\bar{\eta}_{L,2}^{abb} = -\bar{\eta}_{L,2}^{aaa} = \frac{e^4 v_F^2}{\hbar^2 S} \frac{\mathcal{D}(\omega)}{16\omega}, \quad a, b \in \{x, y\}, \quad (17)$$

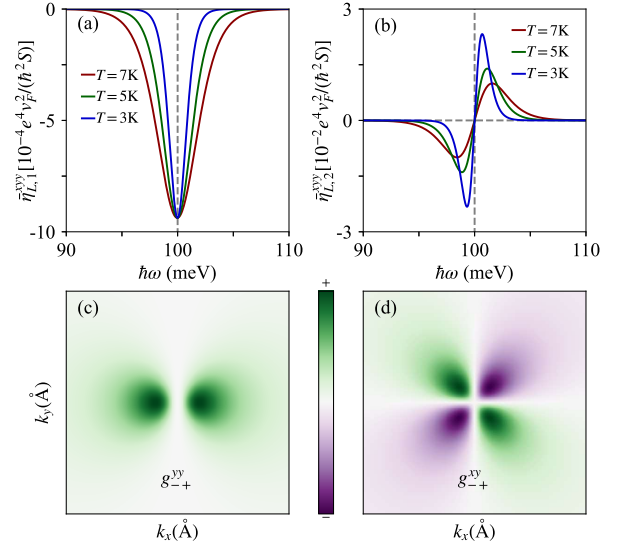


FIG. 2. The temperature and frequency dependencies of (a) $\bar{\eta}_{L,1}^{xyy}$ and (b) $\bar{\eta}_{L,2}^{xyy}$, as calculated in Eqs. (16-17), respectively. Note that the vertical axis between (a) and (b) differs by a factor of 10^2 . Here we have also set $\mu = 50$ meV. The \mathbf{k} -resolved quantum metric (c) g_{-+}^{yy} and (d) g_{-+}^{xy} .

where e , \hbar , and v_F (the Fermi velocity) are restored by dimension analysis and S is the area of the system under investigation.

As expected, the resonant behavior of $\bar{\eta}_{L,1}^{abb/aaa}$ and $\bar{\eta}_{L,2}^{abb/aaa}$, is fully determined by the dimensionless weights $\mathcal{C}(\omega)$ and $\mathcal{D}(\omega)$, respectively, as illustrated in Figs. 2a-2b for the xyy component, in which the corresponding quantum metric are also shown [see Figs. 2c-2d]. While both $\bar{\eta}_{L,1}^{xyy}$ and $\bar{\eta}_{L,2}^{xyy}$ survive as $T \rightarrow 0$, we observe that the peak value of $\bar{\eta}_{L,2}^{xyy}$ is two orders of magnitude larger than that of $\bar{\eta}_{L,1}^{xyy}$ at $T < 10$ K. This difference grows as $T \rightarrow 0$, since the resonant peak of $\bar{\eta}_{L,2}^{xyy}$ scales as $1/T$ whereas the peak value of $\bar{\eta}_{L,1}^{xyy}$ remains intact at $\omega = 2|\mu|$ when $T \rightarrow 0$. Thus, Eq. (14) can be safely neglected at low temperatures (such as $T < 10$ K), and Eq. (15) becomes the dominant contribution to the *anomalous* DTN.

In addition to monolayer graphene, similar physics can be observed in the surface state of 3D topological insulators, which are effectively described by $\mathbf{d} = (-k_y, k_x, 0)$ ²⁴. Since this model has the same dispersion and quantum metric as the monolayer graphene, we arrive at the same physics discussed above. Beyond the linear dispersion, Eq. (6) can also include quadratic terms on \mathbf{k} . For example, it is straightforward to show that the Hamiltonian $H = k^2 + \lambda \mathbf{d} \cdot \boldsymbol{\sigma}$, where \mathbf{d} depends linearly on \mathbf{k} , can also give rise to *anomalous* DTN. This Hamiltonian in general describes three typical 2D systems with spin-orbit coupling (SOC)⁴⁵: (1) Rashba SOC; (2) Dresselhaus SOC; and (3) Weyl SOC.

Anomalous DTN in 3D. — In 3D, we consider the low-energy effective model of Weyl semimetals, described by $\mathbf{d} = (k_x, k_y, k_z)$ near the Weyl node²⁸. For this model,

$\omega_{+-} = 2h$ where $h = (k_x^2 + k_y^2 + k_z^2)^{1/2}$, $v_{\pm}^a = \pm k_a/k$, and $g_{\mp\pm}^{bc} = (k^2\delta_{bc} - k_b k_c)/(2h^4)$. Using these expressions along with Eqs. (14-15) we find

$$\bar{\eta}_{L,1}^{abb} = 2\bar{\eta}_{L,1}^{aaa} = -\frac{e^4 v_F}{\hbar^2 V} \frac{2\mathcal{C}(\omega)}{15\pi}, \quad a, b, c \in \{x, y, z\}, \quad (18)$$

$$\bar{\eta}_{L,2}^{aaa} = -2\bar{\eta}_{L,2}^{abb} = -\frac{e^4 v_F}{\hbar^2 V} \frac{\mathcal{D}(\omega)}{30\pi}, \quad a, b, c \in \{x, y, z\}, \quad (19)$$

which also shows the resonant behavior determined by the dimensionless weights $\mathcal{C}(\omega)$ and $\mathcal{D}(\omega)$, respectively. As a result, both Eq. (18) and Eq. (19) remain valid even at zero temperature, with Eq. (19) becoming the dominant contribution at low temperatures (e.g. $T < 10\text{K}$).

Anomalous DTN versus DSN. — In mesoscopic conductors, the shot noise (SN) dominates over the thermal noise (TN) at low temperatures. This naturally raises a question: Can the *anomalous* DTN be overshadowed by the DSN in bulk crystals even under light illumination? In metallic crystals with time-reversal symmetry, the DSN also consists of two distinct contributions, which, within the two-band limit, are given by^{40,46}:

$$\eta_{L,1}^{abc} = \int_k f_{nm}^2 \Xi_{nm}^{abc} \delta(\omega - \omega_{mn}), \quad (20)$$

$$\eta_{L,2}^{abc} = \int_k \omega \frac{\partial f_{nm}^2}{\partial \epsilon_n} \Lambda_{nm}^{abc} \delta(\omega - \omega_{mn}), \quad (21)$$

where the first term $\eta_{L,1}^{abc}$ with $f_{nm} \equiv f_n - f_m$ stands for the Fermi-sea contribution while the second term $\eta_{L,2}^{abc}$ involving $\partial f_{nm}^2 / \partial \epsilon_n$ accounts for the Fermi-surface contribution.

Similarly, for Eq. (6), by using the optical selection rule $\delta(\omega - \omega_{mn})$ to factorize out the electron occupation information, we similarly obtain

$$\eta_{L,1}^{abc} = \mathcal{C}_1(\omega) \mathcal{N}_1^{abc}, \quad \eta_{L,2}^{abc} = \mathcal{D}_1(\omega) \mathcal{N}_2^{abc}, \quad (22)$$

where $\mathcal{N}_{1/2}^{abc}$ have been defined in Eqs. (14-15), $\mathcal{C}_1(\omega) \equiv f_{-+}^2$ and $\mathcal{D}_1(\omega) \equiv \omega \partial f_{-+}^2 / \partial \epsilon_-$ are also dimensionless weights. Explicitly, they are given by⁴⁰

$$\mathcal{C}_1(\omega) = \frac{\sinh^2(l_1/2)}{[\cosh(l_2) + \cosh(l_1/2)]^2}, \quad (23)$$

$$\mathcal{D}_1(\omega) = -l_1 \frac{2 \sinh(l_1/2) + \sinh(l_1) \cosh(l_2)}{[\cosh(l_2) + \cosh(l_1/2)]^3}, \quad (24)$$

where $l_1 = \hbar\omega/(k_B T)$ and $l_2 = \mu/(k_B T)$ with \hbar and k_B being restored by dimension analysis. By comparing $\mathcal{C}_1(\omega)$ with $\mathcal{D}_1(\omega)$, as shown in Figs. 3a-3b for various temperatures, we find that the Fermi-surface contribution of the DSN is one to two orders of magnitude larger than its Fermi-sea contribution at low temperatures (e.g., $T < 10\text{K}$) since \mathcal{N}_1^{abc} and \mathcal{N}_2^{abc} are of the same order. Therefore, the Fermi-surface contribution becomes the dominant source of the DSN at low temperatures (e.g., $T < 10\text{K}$). Interestingly, we note that the Fermi-surface contribution of DSN also features a $1/T$ divergence, similar to

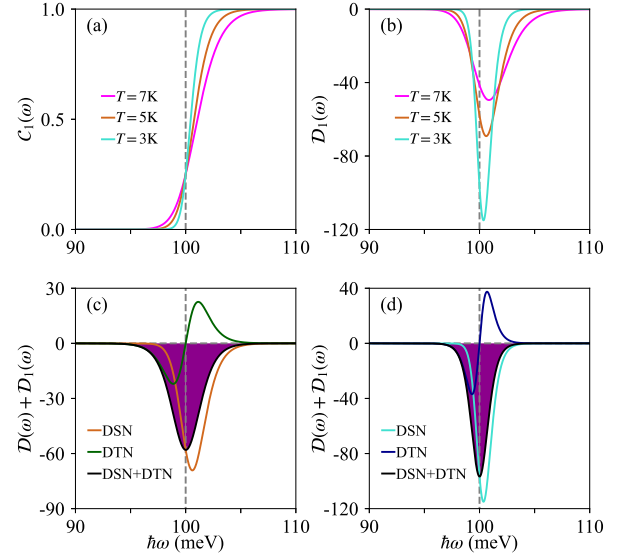


FIG. 3. The temperature and frequency dependencies of (a) $\mathcal{C}_1(\omega)$ and (b) $\mathcal{D}_1(\omega)$, as defined in Eqs. (23-24). The total injection noise spectrum contributed by the *anomalous* DTN and the DSN at (c) $T = 5\text{K}$ and (d) $T = 3\text{K}$.

the second type of *anomalous* DTN. Note that the $1/T$ -DSN can also not be expected in mesoscopic conductors or in bulk crystals under a static electric field.

Further, by comparing Eq. (22) with Eq. (13), we find that the difference between the *anomalous* DTN and the DSN at low temperatures is completely decided by their dimensionless weights [$\mathcal{D}(\omega)$ versus $\mathcal{D}_1(\omega)$]. Essentially, this is because both DSN and DTN are derived from Eq. (3) so that $\eta_{L,1}^{abc}$ and $\eta_{L,2}^{abc}$ can be obtained by replacing \bar{f}_{nm} with f_{nm}^2 in $\bar{\eta}_{L,1}^{abc}$ and $\bar{\eta}_{L,2}^{abc}$, respectively, as adopted in Supplemental Material⁴⁰. Notably, we find that $\mathcal{D}(\omega)$ and $\mathcal{D}_1(\omega)$ are of the same order at a given temperature and therefore the *anomalous* DTN can not be overshadowed by the DSN, as is typically observed in mesoscopic conductors.

Finally, we wish to mention that the resonant behaviors of $\mathcal{D}(\omega)$ and $\mathcal{D}_1(\omega)$ are markedly different. Specifically, $\mathcal{D}_1(\omega)$ exhibits a single resonant peak at the right side of $\omega = 2|\mu|$, whereas $\mathcal{D}(\omega)$ shows resonant peaks on both side of $\omega = 2|\mu|$, particularly in an antisymmetric pattern. As a result, the total injection noise spectrum at low temperatures contributed by both the *anomalous* DTN and the $1/T$ -DSN, which is defined by $\eta_{tot} = [\mathcal{D}(\omega) + \mathcal{D}_1(\omega)] \mathcal{N}_2^{abc}$ universally shows a resonant peak at $\omega_p = 2|\mu|$, as illustrated in Figs. 3c-d for $T = 5\text{K}$ and $T = 3\text{K}$, respectively. Once the total noise spectrum is experimentally measured, the DTN and DSN contributions can be isolated as

$$\bar{\eta}_{L,2} = \frac{\mathcal{D}}{\mathcal{D} + \mathcal{D}_1} \eta_{tot}, \quad \eta_{L,2} = \frac{\mathcal{D}_1}{\mathcal{D} + \mathcal{D}_1} \eta_{tot}, \quad (25)$$

respectively, where \mathcal{D} and \mathcal{D}_1 are dimensionless universal functions decided by the unique electron-photon interaction.

Summary. — We developed the quantum theory of DTN in

bulk crystals under light illumination, demonstrating that in time-reversal-invariant systems, the DTN is closely connected to the quantum metric. Remarkably, the DTN can exhibit a $1/T$ thermal noise *anomaly*, arising from the interplay between the optical selection rule and the inherent Fermi-surface property of DTN. Our findings are illustrated using massless Dirac or Weyl Hamiltonians. Instead of being overshadowed by DSN, the *anomalous* DTN is comparable with the DSN and can lead to a universally resonant behavior of the total noise spectrum at low temperatures. We wish to remark that the shot noise generated by nonequilibrium electrons will produce fluctuating electromagnetic evanescent fields at the surface of the material. These fields can be detected non-

invasively using the scanning noise microscope^{47,48}, without the need for metallic electrodes typically used in mesoscopic measurements^{49,50}. These experimental progresses provide a potential pathway to verify our proposals in Dirac materials.

ACKNOWLEDGEMENTS

This work was financially supported by the Natural Science Foundation of China (Grants No.12034014, No.12474047, and No.12174231.)

-
- * zhanglei@sxu.edu.cn
† jianwang@hku.hk
- ¹ S. Datta, *Electronic Transport in Mesoscopic Systems* (Cambridge University Press, 1997).
 - ² S. Datta, *Quantum Transport: atom to transistor* (Cambridge University Press, 2005).
 - ³ Ya. M. Blanter and M. Buttiker, *Shot noise in mesoscopic conductors*, *Phys. Rep.* **1**, 336 (2000).
 - ⁴ C. Beenakker and C. Schönberger, *Quantum Shot Noise*, *Phys. Today* **56**, 37 (2003).
 - ⁵ H. Nyquist, *Thermal Agitation of Electric Charge in Conductors*, *Phys. Rev.* **32**, 110 (1928).
 - ⁶ T. Neupert, C. Chamon, and C. Mudry, *Measuring the quantum geometry of Bloch bands with current noise*, *Phys. Rev. B* **87**, 245103 (2013).
 - ⁷ M. M. Wei, L. Y. Wang, B. Wang, L. J. Xiang, F. M. Xu, B. G. Wang, and J. Wang, *Quantum Fluctuation of the Quantum Geometric Tensor and Its Manifestation as Intrinsic Hall Signatures in Time-Reversal Invariant Systems*, *Phys. Rev. Lett.* **130**, 036202 (2023).
 - ⁸ T. Morimoto, M. Nakamura, M. Kawasaki, and N. Nagaosa, *Current-Voltage Characteristic and Shot Noise of Shift Current Photovoltaics*, *Phys. Rev. Lett.* **121**, 267401 (2018).
 - ⁹ L. J. Xiang, H. Jin, and J. Wang, *Quantifying the photocurrent fluctuation in quantum materials by shot noise*, *Nat. Commun.* **15**, 2012 (2024).
 - ¹⁰ C. Wang, Y. Gao, and D. Xiao, *Intrinsic nonlinear Hall effect in antiferromagnetic tetragonal CuMnAs*, *Phys. Rev. Lett.* **127**, 277201 (2021).
 - ¹¹ H. Liu, J. Zhao, Y.-X. Huang, W. Wu, X.-L. Sheng, C. Xiao, and S. Y. A. Yang, *Intrinsic second-order anomalous Hall effect and its application in compensated antiferromagnets*, *Phys. Rev. Lett.* **127**, 277202 (2021).
 - ¹² A. Gao, Y.-F. Liu, J.-X. Qiu, B. Ghosh, T. V. Trevisan, Y. Onishi, C. Hu, T. Qian, H.-J. Tien, S.-W. Chen, *et al.*, *Quantum metric nonlinear Hall effect in a topological antiferromagnetic heterostructure*, *Science* **381**, 181 (2023).
 - ¹³ N. Wang, D. Kaplan, Z. Zhang, T. Holder, N. Cao, A. Wang, X. Zhou, F. Zhou, Z. Jiang, C. Zhang *et al.*, *Quantum-metric-induced nonlinear transport in a topological antiferromagnet*, *Nature (London)* **621**, 487 (2023).
 - ¹⁴ L. Wang, J. Zhu, H. Chen, H. Wang, J. Liu, Y.-X. Huang, B. Jiang, J. Zhao, H. Shi, G. Tian, H. Wang, Y.-G. Yao, D.-P. Yu, Z. Wang, C. Xiao, S. Y. A. Yang, and X. S. Wu, *Orbital magneto-nonlinear anomalous Hall effect in kagome magnet Fe_3Sn_2* , *Phys. Rev. Lett.* **132**, 106601 (2024).
 - ¹⁵ L.-J. Xiang and J. Wang, *Intrinsic in-plane magnetononlinear Hall effect in tilted Weyl semimetals*, *Phys. Rev. B* **109**, 075419 (2024).
 - ¹⁶ J. Han, T. Uchimura, Y. Araki, J.-Y. Yoon, Y. Takeuchi, Y. Yamane, S. Kanai, J. Ieda, H. Ohno, and S. Fukami, *Room-temperature flexible manipulation of the quantum-metric structure in a topological chiral antiferromagnet*, *Nat. Phys.* **20**, 1110 (2024).
 - ¹⁷ J. X. Jia, L. J. Xiang, Z. H. Qiao, and J. Wang, *Equivalence of semiclassical and response theories for second-order nonlinear ac Hall effects*, *Phys. Rev. B* **110**, 245406 (2024).
 - ¹⁸ K. S. Novoselov, A. K. Geim, S. V. Morozov, D. Jiang, Y. Zhang, S. V. Dubonos, I. V. Grigorieva, A. A. Firsov, *Electric Field Effect in Atomically Thin Carbon Films*, *Science* **306**, 666 (2004).
 - ¹⁹ Y. B. Zhang, Y.-W. Tan, H. L. Stormer, and P. Kim, *Experimental observation of the quantum Hall effect and Berry's phase in graphene*, *Nature* **438**, 201 (2005).
 - ²⁰ A. K. Geim, K. S. Novoselov, *The rise of graphene*, *Nat. Mater.* **6**, 183 (2007).
 - ²¹ D. Xiao, W. Yao, and Q. Niu, *Valley-Contrasting Physics in Graphene: Magnetic Moment and Topological Transport*, *Phys. Rev. Lett.* **99**, 236809 (2007).
 - ²² H. J. Zhang, C.-X. Liu, X.-L. Qi, X. Dai, Z. Fang, and S.-C. Zhang, *Topological insulators in Bi_2Se_3 , Bi_2Te_3 and Sb_2Te_3 with a single Dirac cone on the surface*, *Nat. Phys.* **5**, 438 (2009).
 - ²³ C.-X. Liu, X.-L. Qi, H. J. Zhang, X. Dai, Z. Fang, and S.-C. Zhang, *Model Hamiltonian for topological insulators*, *Phys. Rev. B* **82**, 045122 (2010).
 - ²⁴ L. Fu, *Hexagonal Warping Effects in the Surface States of the Topological Insulator Bi_2Te_3* , *Phys. Rev. Lett.* **103**, 266801 (2009).
 - ²⁵ M. Z. Hasan and C. L. Kane, *Colloquium: Topological insulators*, *Rev. Mod. Phys.* **82**, 3045 (2010).
 - ²⁶ X.-L. Qi and S.-C. Zhang, *Topological insulators and superconductors*, *Rev. Mod. Phys.* **83**, 1057 (2011).
 - ²⁷ J. E. Moore, *The birth of topological insulators*, *Nature* **464**, 194 (2010).
 - ²⁸ N. P. Armitage, E. J. Mele, and A. Vishwanath, *Weyl and Dirac semimetals in three-dimensional solids*, *Rev. Mod. Phys.* **90**, 015001 (2018).
 - ²⁹ B. Q. Lv, T. Qian, and H. Ding, *Experimental perspective on three-dimensional topological semimetals*, *Rev. Mod. Phys.* **93**, 025002 (2021).

- ³⁰ B. H. Yan and C. Felser, *Topological Materials: Weyl Semimetals*, *Ann. Rev. Condens. Matt. Phys.* **8**, 337 (2017).
- ³¹ Note that $f_\alpha(1 - f_\alpha) = -T\partial f_\alpha/\partial E = -Tf'_\alpha$.
- ³² F. D. M. Haldane, *Berry Curvature on the Fermi Surface: Anomalous Hall Effect as a Topological Fermi-Liquid Property*, *Phys. Rev. Lett.* **93**, 206602 (2004).
- ³³ J. E. Sipe and A. I. Shkrebti, *Second-order optical response in semiconductors*, *Phys. Rev. B* **61**, 5337 (2000).
- ³⁴ D. Xiao, M.C. Chang, and Q. Niu, *Berry phase effects on electronic properties*, *Rev. Mod. Phys.* **82**, 1959 (2010).
- ³⁵ T. Morimoto and N. Nagaosa, *Topological Nature of Nonlinear Optical Effects in Solids*, *Sci. Adv.* **2**, e1501524 (2016).
- ³⁶ The optical selection rule dictates that the incident light frequency ω must match the energy difference $\hbar\omega_{nm} = \epsilon_n - \epsilon_m$ between the n th band and the m th one to allow the optical transition.
- ³⁷ S. Q. Shen, *Topological Insulators* (Springer-Verlag, Berlin Heidelberg, 2012).
- ³⁸ O. Vafek and A. Vishwanath, *Dirac Fermions in Solids: From High-Tc Cuprates and Graphene to Topological Insulators and Weyl Semimetals*, *Annu. Rev. Condens. Matt. Phys.* **5**, 83 (2014).
- ³⁹ Note that $\epsilon_\pm = \pm d = \pm\omega/2$.
- ⁴⁰ Supplemental Material. (I) The calculations of \mathcal{C}^\pm , \mathcal{D}^\pm , \mathcal{C}_1 , and \mathcal{D}_1 . (II) The DC noise theory in metallic bulk systems. (III) The shift DTN for the massless Dirac model.
- ⁴¹ H. Wang and X. F. Qian, *Electrically and magnetically switchable nonlinear photocurrent in \mathcal{PT} -symmetric magnetic topological quantum materials*, *npj Comput. Mater.* **6**, 199 (2020).
- ⁴² A. M. Cook, B. M. Fregoso, F. de Juan, S. Coh, and Joel E. Moore, *Design principles for shift current photovoltaics*, *Nat. Commun.* **8**, 14176 (2017).
- ⁴³ As a comparison, we wish to remark that the shift and injection DTNs, excited by LPL and CPL, respectively, are related to the local Berry curvature defined by $\Omega_{nm}^{bc} = i(r_{nm}^b r_{mn}^c - r_{nm}^c r_{mn}^b)$ and the group velocity difference Δ_{nm}^a defined in Eqs. (11-12), in a way of $\Delta_{nm}^a (\Omega_{nm}^{ab} \Delta_{mn}^c + \Omega_{nm}^{ac} \Delta_{mn}^b)$ and $(\Delta_{nm}^a)^2 \Omega_{nm}^{bc}$.
- ⁴⁴ P. Törmä, *Essay: Where Can Quantum Geometry Lead Us?*, *Phys. Rev. Lett.* **131**, 240001 (2023).
- ⁴⁵ L. L. Tao and E. Y. Tsymbal, *Persistent spin texture enforced by symmetry*, *Nat. Commun.* **9**, 2763 (2018).
- ⁴⁶ We use $\tilde{\eta}$ and η to denote, respectively, the injection DTN and DSN.
- ⁴⁷ Q. C. Weng, S. Komiyama, L. Yang, Z. H. An, P. P. Chen, S.-A. Biehs, Y. Kajihara, W. Lu, *Imaging of nonlocal hot-electron energy dissipation via shot noise*, *Science*. **360**, 775 (2018).
- ⁴⁸ Q. C. Weng, L. Yang, Z. H. An, P. P. Chen, A. Tzalenchuk, W. Lu, and S. Komiyama, *Quasiadiabatic electron transport in room temperature nanoelectronic devices induced by hot-phonon bottleneck*, *Nat. Commun.* **12**, 4752 (2021).
- ⁴⁹ L. DiCarlo, Y. Zhang, D. T. McClure, C. M. Marcus, L. N. Pfeiffer, and K. W. West, *System for measuring auto- and cross correlation of current noise at low temperatures*, *Rev. Sci. Instrum.* **77**, 073906 (2006).
- ⁵⁰ I. Tamir, V. Caspari, D. Rolf, C. Lotze, and K. J. Franke, *Shot-noise measurements of single-atom junctions using a scanning tunneling microscope*, *Rev. Sci. Instrum.* **93**, 023702 (2022).